RESEARCH ARTICLE

LITHIUM EXTRACTION

# Lithium extraction from brine through a decoupled and membrane-free electrochemical cell design

Zhen Li, I-Chun Chen, Li Cao, Xiaowei Liu, Kuo-Wei Huang*, Zhiping Lai*

**The sustainability of lithium-based energy storage or conversion systems, e.g., lithium-ion batteries, can be enhanced by establishing methods of efficient lithium extraction from harsh brines. In this work, we describe a decoupled membrane-free electrochemical cell that cycles lithium ions between iron-phosphate electrodes and features cathode (brine) and anode (fresh water) compartments that are isolated from each other yet electrochemically connected through a pair of silver/silver-halide redox electrodes. This design is compatible with harsh brines having magnesium/lithium molar ratios of up to 3258 and lithium concentrations down to 0.15 millimolar, enabling the production of battery-grade (>99.95% pure) lithium carbonate. Energy savings of up to ~21.5% were realized by efficiently harvesting the osmotic energy of the brines. A pilot-scale cell with an electrode surface area of 33.75 square meters was used to realize lithium extraction from Dead Sea brine with a recovery rate of 84.0%.**

Lithium is an indispensable component of high-performance batteries widely used in portable electronic devices, electric vehicles, and renewable energy systems (*1*–*4*). Given that the conventional global lithium reserves (~22 million tons) (*5*) are expected to be used up by 2080 (*6*, *7*), considerable attention has been drawn to the utilization of unconventional lithium sources, including inferior brines and seawater, which contain >230 billion tons of lithium. However, this lithium cannot be extracted by the conventional soda-lime evaporation method because of the low concentration of lithium and high levels of interfering ions (*8*). Traditional extraction methods also cause substantial water loss, escalating the already intense water scarcity in arid areas and causing severe environmental pollution owing to the use of toxic chemicals. Therefore, numerous works have focused on establishing direct (i.e., additive-free) lithium extraction technologies, particularly electrical field–assisted ones, as they enable the rapid extraction of lithium from inferior brines (those with lithium concentrations of <15 mM) (*9*–*11*). For example, the recently developed rocking chair method relies on electrochemical lithium extraction in a two-compartment reactor divided by an anion-exchange membrane, integrating adsorption and desorption processes (*12*–*16*). In these processes, process efficiency is heavily reliant on membrane performance. However, the commercial anion-exchange membranes used in the rocking chair process typically have poor ion selectivity, which causes severe ion backmixing and incompatibility with harsh brines (those with high Mg/Li ratios and/or low lithium concentrations). Our group has developed an electrodialysis process using a lithium-containing inorganic solid electrolyte as a membrane to increase the lithium content of seawater from ~0.03 to 1300 mM (*17*). In this case, the utilized membranes show superior ion selectivity but suffer from low flux.

The high salinity of most inferior lithium brines creates a substantial osmotic potential between the brine and lithium extraction solution. This potential, ubiquitously observed upon the contact of seawater and river (fresh) water, is the origin of the so-called "blue energy," which is ranked as the second-largest marine-based energy source (1.4 to 2.6 TW) (*18*, *19*) and can potentially be harvested using membrane-based methods, such as pressure-retarded osmosis and reverse electrodialysis. However, existing membranes suffer from suboptimal separation performance, as exemplified by the low power density (<5.0 W $m^{-2}$) achieved by using commercial membranes in seawater and river water systems (*20*–*22*). Although the recent development of advanced materials, such as graphene, carbon nanotubes, and covalent organic frameworks, has enabled the realization of power densities of up to 200 W $m^{-2}$, they have been demonstrated only for square micrometer–scale membrane areas, decreasing to 4.0 to 14.6 W $m^{-2}$ with a membrane area increase to the square millimeter scale (*23*, *24*). Furthermore, the prevention of fouling, which is the weakness of membrane technology, requires expensive brine pretreatment that may completely offset the benefit of osmotic energy harvesting (*23*).

Cronin *et al.* proposed the concept of decoupled electrolysis using soluble polyoxometalates as intermediary redox electrolyte pairs (*25*), whereas Grader *et al.* improved the system using a solid NiOH-NiOOH electrolyte pair (*26*) and showed that the decoupled system could harness thermal energy when the two chambers were held at different temperatures (*27*). Inspired by these works, we developed a membrane-free decoupled electrochemical process to overcome the abovementioned limitations and realized the extraction of lithium from harsh brines with lithium concentrations of down to ~0.15 mM (i.e., 1 ppm) while utilizing the osmotic potential to substantially reduce energy consumption.

## Design of the decoupled membrane-free lithium extraction cell

In the decoupled membrane-free (DCMF) cell used for lithium extraction (Fig. 1A), the cathode compartment (brine feed) and anode compartment (extraction solution) were physically isolated from each other but electrochemically connected through a pair of working ($FePO_4$/$LiFePO_4$) and redox (Ag/AgX) electrodes. The X in silver halide was either Cl or Br, as chloride and bromide are the primary anions in natural lithium brines. The two pairs of electrodes were fabricated as flat sheets of the same size to accelerate mass transport and reduce the interfacial resistance. In the cathode compartment, the $Li^+$ ions from the feed solution (brine) were intercalated into the framework of $FePO_4$,

**Table 1. Compositions of the studied brines.***

| Samples | Li (mM) | Na (mM) | K (mM) | Mg (mM) | Ca (mM) | Cl (mM) | Br (mM) |
|---|---|---|---|---|---|---|---|
| Solution 5 | 11.64 | 215.05 | 120.89 | 2313.33 | 587.13 | 6148.50 | 0 |
| Solution 4 | 6.08 | 215.05 | 120.89 | 2313.33 | 587.13 | 6142.94 | 0 |
| Solution 3 | 2.77 | 215.05 | 120.89 | 2313.33 | 587.13 | 6139.63 | 0 |
| Solution 2 | 1.42 | 215.05 | 120.89 | 2313.33 | 587.13 | 6138.28 | 0 |
| Solution 1 | 0.71 | 215.05 | 120.89 | 2313.33 | 587.13 | 6137.57 | 0 |
| Natural brine† | 6.73 | 73.75 | 34.69 | 2681.85 | 614.13 | 6599.03 | 108.1 |

*Ion concentration was determined by using ICP-OES. †Natural brine (Dead Sea water) was collected from the Dead Sea within the Jordan area and used without further purification.

Division of Physical Science and Engineering, King Abdullah University of Science and Technology (KAUST), Thuwal 23955-6900, Kingdom of Saudi Arabia.
*Corresponding author. Email: kuowei.huang@kaust.edu.sa (K.-W.H.); zhiping.lai@kaust.edu.sa (Z.L.)

which was gradually converted to $LiFePO_4$ (Eq. 1), whereas the $X^-$ anions formed AgX on the oxidized silver surface (Eq. 2). In the anode compartment, the $LiFePO_4$ electrode released $Li^+$ ions to the extraction solution upon oxidative conversion to $FePO_4$ (Eq. 3), whereas the AgX electrode released $X^-$ upon the reductive plating of Ag (Eq. 4). The overall reaction corresponded to the extraction of LiX from the feed (Eq. 5). In Eqs. 1 to 4, $e^-$ represents the transferred electron in the redox reactions.

***Cathode compartment***

$$FePO_4 \text{ electrode: } FePO_4 + Li^+ + e^- \rightleftharpoons LiFePO_4 \quad (1)$$

$$\text{Ag electrode: } Ag + X^-_{(feed)} \rightleftharpoons AgX + e^- \quad (2)$$

***Anode compartment***

$$LiFePO_4 \text{ electrode: } LiFePO_4 \rightleftharpoons FePO_4 + Li^+_{(extraction)} + e^- \quad (3)$$

$$\text{AgX electrode: } AgX + e^- \rightleftharpoons Ag + X^-_{(extraction)} \quad (4)$$

***Overall reaction***

$$Li^+_{(feed)} + X^-_{(feed)} \rightleftharpoons Li^+_{(extraction)} + X^-_{(extraction)} \quad (5)$$

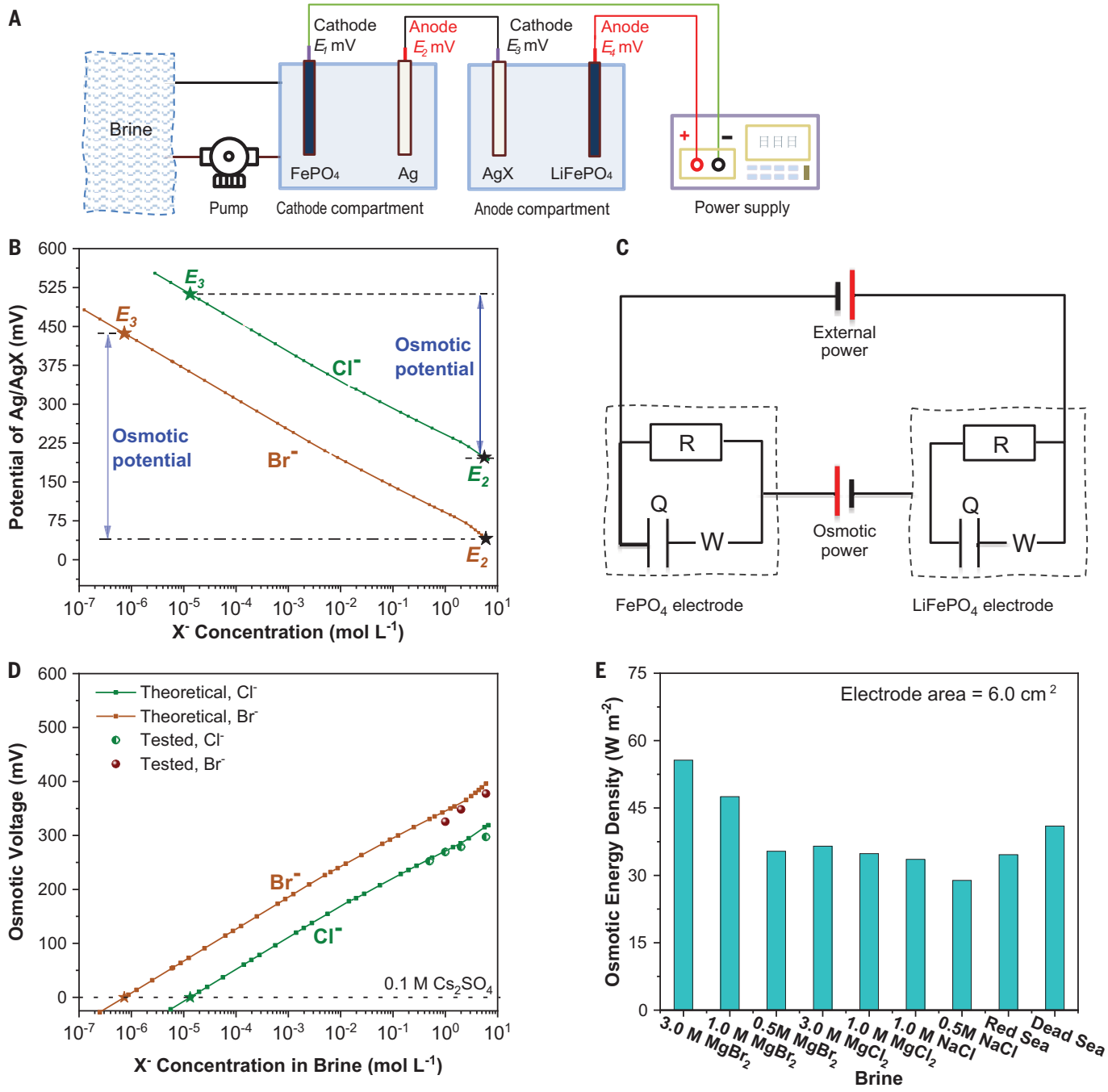


**Fig. 1. Blue energy–assisted electrochemical lithium extraction.** (**A**) Design of the DCMF cell. (**B**) Theoretical dependence of the Ag/AgX electrode potential on the concentration of $X^-$. (**C**) Equivalent circuit diagram of the setup in (A), with *R*, *C*, and *W* denoting electrical, capacitive, and Warburg resistances, respectively. The osmotic potential generated on the Ag/AgX electrodes is equivalent to an internal power source. (**D**) Osmotic voltages on the Ag/AgX electrodes measured at different $X^-$ concentrations and comparison with theoretical values. (**E**) Density of osmotic energy harvested by the DCMF system (electrode surface area = 6.0 $cm^2$) in different brines.

When the reactions in the cathode and anode compartments almost reached equilibrium, the positions of the two electrode pairs were switched to recover their original electrochemical configurations and allow the reactions to continue. As a result, the $Li^+$ ions were continuously transferred from the feed solution to the extraction solution with the aid of the $FePO_4$/$LiFePO_4$ electrode, whereas halide anions were shifted from the feed solution to the extraction solution through the mediation of the Ag/AgX electrode.

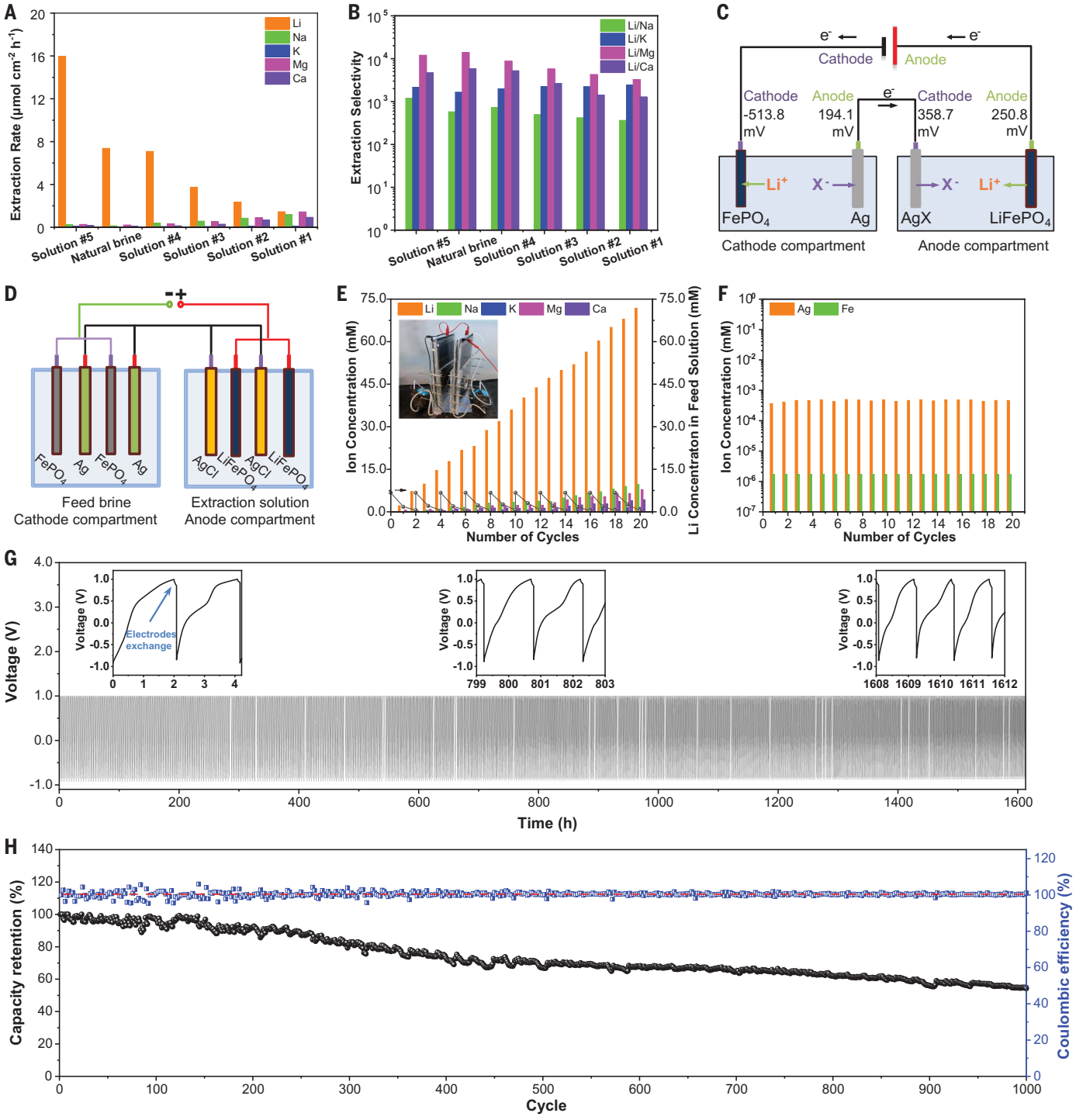


**Fig. 2. Lithium extraction performance of the bench-scale DCMF cell.** Average extraction rates (**A**) and ion extraction selectivities (**B**) obtained for different feed brines. (**C**) Electrode potential distribution during lithium extraction from natural brine. (**D**) Illustration of the DCMF system with two assemblies of electrodes. (**E**) Evolution of the ion concentration in the extraction solution and lithium concentration in the remaining feed solution during cycling. (**F**) Evolution of silver and iron concentrations in the extraction solution during cycling. (**G**) Polarization curves of the DCMF system recorded over 1000 cycles. The diagram shows only the electrochemical process in the cathode compartment. The process in the anode compartment should show the reverse. (**H**) Evolution of the capacity retention and coulombic efficiency of the DCMF system over 1000 cycles.

Osmotic energy harvesting is based on the strong dependence of the Ag/AgX electrode potential on the concentration of $X^-$ (Eq. 6 and Fig. 1B).

$$Ag + X^- \rightleftharpoons AgX + e^-, E_{Ag/AgX} = E^0_{Ag/AgX} - 0.05916\log(a_x)(25°C) \quad (6)$$

$$U_{osmotic} = -0.05916\log\left(\frac{a_{X,extraction}}{a_{X,feed}}\right)(25°C) \quad (7)$$

Here, $a_x$ is the activity of $X^-$, $E_{Ag/AgX}$ is the electrode potential of Ag/AgX in volts, and $U_{osmotic}$ is the osmotic potential in volts (*28*, *29*). Given that the brine feed had a notably higher concentration of $X^-$ than the extraction solution, an osmotic voltage was generated on the Ag/AgX electrodes, serving as an internal driving force for electrochemical reactions (Fig. 1C).

To verify the possibility of osmotic energy harvesting, we designed a symmetrical cell (fig. S1) in which the working electrode pair was replaced by two equipotential probes, and the power supply was replaced by a passive electronic load. Because no external power source was used, the detected power output originated from osmotic energy. As shown in Fig. 1D, when 1.0 to 6.0 M $Br^-$, 0.5 to 6.0 M $Cl^-$, real Red Sea water, and real Dead Sea water were used as the feed solutions, open-circuit potentials of 325.6 to 377.5, 252.3 to 294.2, 272.5, and 324.9 mV were detected, respectively, well matching the theoretical values calculated with Eq. 7. The respective peak power densities achieved on the Ag/AgX electrode were 35.38 to 55.65, 28.89 to 36.51, 34.61, and 40.97 W $m^{-2}$ (Fig. 1E), exceeding the values previously reported for other membrane systems of practical sizes (table S1).

**Lithium extraction performance**

The $FePO_4$ electrode sorbs $Li^+$ in preference to other ions. This behavior can be explained by considering the corresponding intercalation potentials, which were measured using the three-electrode device depicted in fig. S2. Values of −17.5, −158.1, −68.8, and −139.0 mV versus the standard hydrogen electrode (SHE) were obtained for $Na^+$, $K^+$, $Mg^{2+}$, and $Ca^{2+}$, respectively, whereas values of 223.0 to 298.2 mV versus SHE were obtained for $Li^+$ in the range of 0.7 to 12 mM (fig. S3). Given that ion intercalation into the $FePO_4$ electrode involves the reduction of $Fe^{3+}$ to $Fe^{2+}$, the high intercalation potential of $Li^+$, even at the lowest concentration studied, indicates that the sorption of $Li^+$ by the $FePO_4$ framework is thermodynamically favored over that of other ions.

Lithium extraction from artificial and natural brines was initially investigated by using a bench-scale DCMF cell with an electrode surface area of 6.00 $cm^2$ ($FePO_4$ loading, 10 mg $cm^{-2}$; Ag loading, 15 mg $cm^{-2}$) and cathode and anode compartment volumes of 75.0 mL. To avoid the introduction of exogenous lithium, the initial $LiFePO_4$ electrode was generated from the $FePO_4$ electrode by using a feed solution (materials and methods). Table 1 lists the compositions of the artificial and natural (Dead Sea) brines used. In these brines, the concentrations of $Na^+$, $K^+$, $Mg^{2+}$, and $Ca^{2+}$ were constant, whereas that of $Li^+$ varied from 0.71 to 11.64 mM (4.92 to 80.79 ppm), and the Mg/Li molar ratio ranged from 198.7 to 3258.2. Compared with those of typical brines (table S2), the total dissolved solid (TDS) contents of our brines were among the highest (~330 g $L^{-1}$), whereas the $Li^+$ ion concentrations were the lowest (~40 versus hundreds to thousands parts per million). Thus, lithium extraction from our brines was more challenging than that from typical brines.

Extraction was performed under a constant external voltage (0.6 V) for 2 hours. In each test, the current decreased with time, as shown in fig. S4, similar to the charging process of a lithium-ion battery. Therefore, the time-weighted electrode area–normalized average lithium extraction rate was used as a performance metric, ranging from 15.96 to 1.44 μmol ($Li^+$) $cm^{-2}$ $h^{-1}$ at lithium concentrations of 11.64 to 0.71 mM, respectively (Fig. 2A). The selectivities of lithium extraction over sodium, potassium, magnesium, and calcium extraction were 361 to 1175, 2133 to 2396, 3247 to 11987, and 1271 to 4648, respectively (Fig. 2B). The performance of the actual brine well matched that of the artificial brines based on lithium concentration, which indicated that the extraction performance was mainly determined by the lithium concentration of the feed solution. These extraction performances exceeded those of the previously reported rocking-chair processes (tables S3 and S4).

The contribution of osmotic energy during extraction was measured by using natural brine and the setup shown in fig. S5, with the potential of each electrode (fig. S6) measured in situ by electrochemical workstations with saturated calomel electrodes as references. Fig. 2C shows the distribution of the average potentials on the $FePO_4$, Ag, AgCl, and $LiFePO_4$ electrodes. A voltage of about +164.6 mV was generated over the cathodic Ag electrode versus the anodic AgCl electrode, and an average current density of 0.90 A $m^{-2}$ was achieved. Given that the external voltage equaled 0.6 V, osmotic energy accounted for 21.5% (148.14 mW $cm^{-2}$) of the overall energy consumption. This energy would otherwise have to be provided by the power supply to drive the process under the same conditions and therefore corresponds to the amount of energy saved.

Another bench-scale DCMF unit with two electrode assemblies (four electrodes for each assembly) was designed for long-term studies, as shown in Fig. 2D. Each electrode was coated by active materials with an area of 45.0 × 25.0 $cm^2$ and a loading rate of 10 mg $cm^{-2}$, as shown in the inset of Fig. 2E as well as fig. S7. The volumes of cathode and anode compartments were 1.35 and 1.60 L, respectively. The extraction voltage and cycle duration were set to 0.6 V and 2 hours, respectively. Extraction was conducted over 20 cycles, and the electrode leaching rate was estimated by measuring the accumulated iron and silver contents of the extraction solution (Fig. 2F) as markers of degradation to the $FePO_4$/$LiFePO_4$ and Ag/AgCl electrodes, respectively. The iron content was below the detection limit of inductively coupled plasma–optical emission spectrometry (ICP-OES; <1.78 nM), and the silver content was determined to be 0.05 ppm (i.e., 0.46 μM). The latter value was 156,000 times less than the accumulated lithium concentration and

**Table 2. Energy costs* of producing 1.0 kg of $Li_2CO_3$ with the pilot-scale DCMF system.**

| Items | | Energy consumption (kWh) | Total energy consumption (kWh) | Proportion (%) |
|---|---|---|---|---|
| Solution transportation (loading and unloading the feed, extraction, and rinse solutions) | | 0.63 | 0.63 | 5.43 |
| Lithium extraction (taking ohmic consumption and power supply efficiency into account) | | 0.57 | 0.57 | 4.90 |
| Electrode exchange | Electrode elevation | 0.53 | 0.77 | 6.68 |
| | Electrode rotation | 0.062 | | |
| | Electrode return | 0.18 | | |
| Rinse and drain | Water washing | 0.95 | 4.39 | 37.88 |
| | Fan-assisted draining | 3.44 | | |
| Control system | PLC | 3.11 | 5.23 | 45.11 |
| | Monitor | 2.12 | | |
| Total | | | 11.59 | 100 |

*The values were calculated from the energy consumption data in table S5 and production rate of 3.175 kg per 112 cycles.

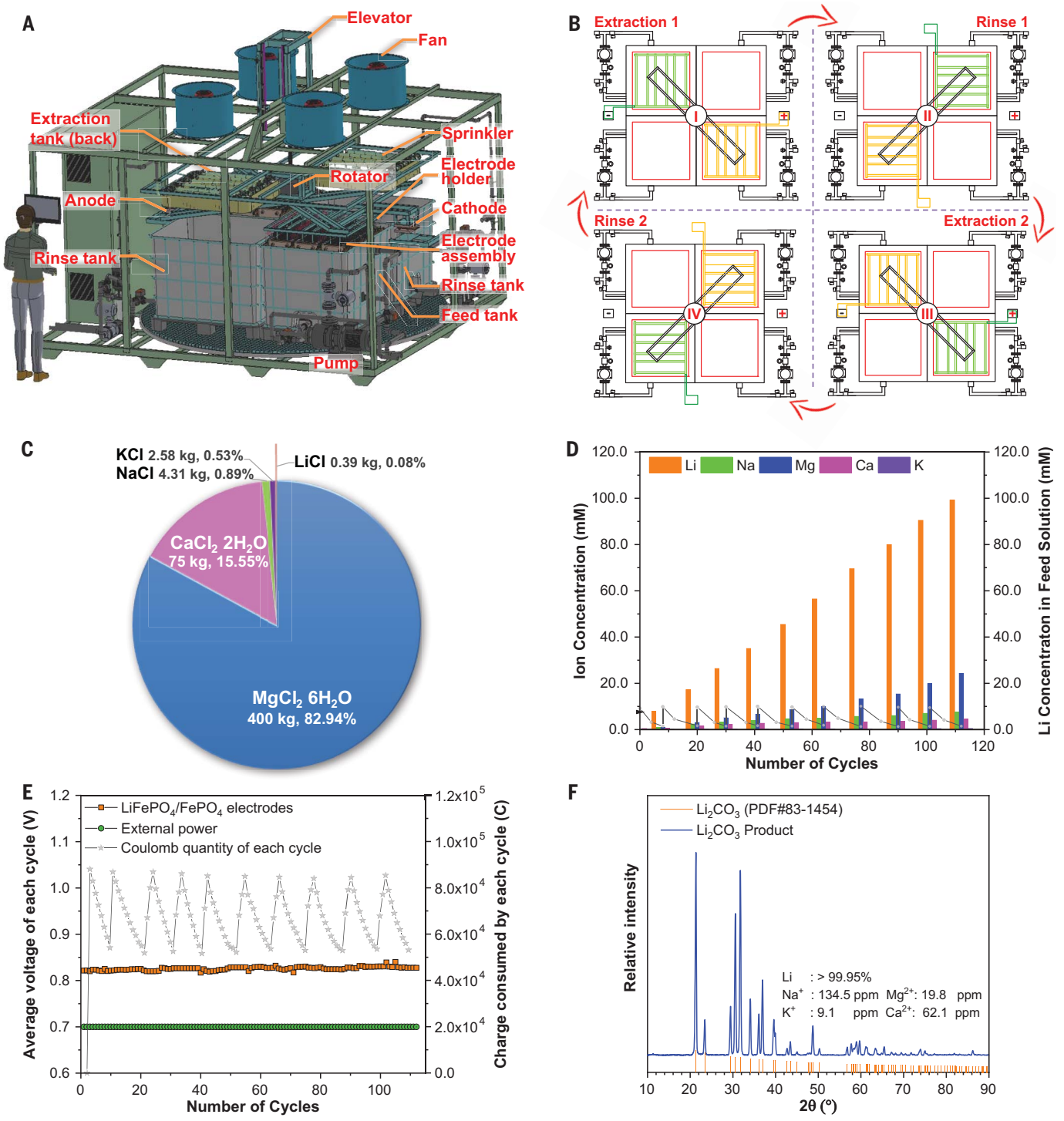


**Fig. 3. Lithium extraction performance of the pilot-scale DCMF process.** (**A**) Illustration and (**B**) operation sequence of the pilot-scale DCMF apparatus. In position I (Extraction 1), the $FePO_4$ and $LiFePO_4$ electrodes in the green and yellow electrode assemblies are connected to the anode and cathode of the external power supply, respectively, with contact pins. The Ag and AgCl electrodes in the green and yellow electrode assemblies are connected to each other. In position II (Rinse 1), all electrodes are lifted out from the tanks and rotated 90°. The contact pins are disconnected from the external power for a rinse. In position III (Extraction 2), all electrodes are lifted out of the rinse tanks and rotated 90°. The contact pins are connected to the external power, but the positions of the green and yellow electrode assemblies are exchanged with each other. In position IV (Rinse 2), all electrodes are lifted out of the tanks and rotated 90° to conduct another rinse step. These steps are conducted sequentially and periodically. (**C**) Composition of 1 ton of Dead Sea brine. (**D**) Evolution of ion concentrations in the extraction solution and lithium concentration in the feed solution during cycling. (**E**) Voltage between $LiFePO_4$/$FePO_4$ electrodes, the applied potential, and amount of charge calculated by integrating the current-time curve during extraction. (**F**) X-ray diffraction patterns of the produced and standard $Li_2CO_3$ together with the results of elemental analysis.

was therefore neglected. The low leaching rate of Ag was attributed to two factors. First, based on the solubilities of AgCl and AgBr estimated from their solubility product ($K_{sp}$) values ($1.78 \times 10^{-10}$ and $5.35 \times 10^{-13}$, respectively), the concentration of the dissolved silver should be of the order of nano- to micromolar (*30*, *31*). Second, the high–surface area (1400 $m^2\ g^{-1}$) activated carbon in the electrode could act as a sorbent for $Ag^+$ immobilization. In addition, the lithium concentration in the brine feed decreased from 6.73 mM (~46.93 ppm) to 0.5 mM (~3.48 ppm) after two cycles, whereas the lithium concentration in the extraction solution concomitantly increased from 0 to 7.19 mM. Accounting for the volume disparity between the cathode compartment (1.6 L) and the anode compartment (1.35 L), the adsorbed and released amounts of lithium agree with the matter conservation. The brine feed was replaced whenever the lithium concentration was decreased to ~0.5 mM (i.e., every two cycles in this test), but the extraction solution was replaced after 20 cycles in which the lithium concentration was eventually increased to 71.82 mM (Fig. 2E). A lithium recovery ratio of 92.6% was obtained.

Fig. 2, G and H, shows the results of long-term durability testing performed over >1600 hours using natural brine. To maintain roughly constant feed and extraction solution concentrations, we connected the cathode and anode compartments to two 2.0-L tanks. Extraction was conducted at a constant current density of 2.5 mA $cm^{-2}$ (based on the electrode surface area) and a cutoff voltage of 1.0 V. When the cutoff voltage was reached, the electrodes were removed, rinsed with deionized water, and returned to opposite positions (anode to cathode and vice versa). As shown in the inset of Fig. 2G, the charge curve for each cycle was highly reproducible for >1000 cycles. The cycle time initially equaled ~2 hours and gradually decreased to 1.5 hours because of capacity reduction. The coulombic efficiency, defined as the capacity of one cycle versus that of the next cycle, was close to 100% throughout the experiment (Fig. 2H). The adsorption capacity of the $FePO_4$/$LiFePO_4$ electrode steadily decreased, with capacity retentions of >91 and 55% observed after 200 and 1000 cycles, respectively. The average capacity loss was ~0.044% per cycle. These results indicate the high upscaling potential of our method.

### Pilot-scale prototype

A pilot-scale DCMF system ~100,000 times larger than the bench-scale setup was used to produce $Li_2CO_3$ powder. An automatic device with dimensions of 3.8 × 3.0 × 2.5 m (length × width × height) was built based on the blueprint in Fig. 3A (see also fig. S8 and movies S1 and S2). The electrode assemblies had a total surface area of 45.0 cm × 25.0 cm × 300 (33.75 $m^2$, length × width × number of electrodes). The apparatus had four square tanks with similar volumes (1.0 $m^3$) combined into a larger square. The cathode and anode compartments were located across one diagonal position, and the two rinse tanks were located on the other diagonal. The positions of the two pairs of electrodes could be switched by simple rotation (by using a lifter and stepping motor), as shown in Fig. 3B, to recover their original electrochemical configurations and allow the reactions to continue. The extraction process was divided into five unit operations orchestrated by a Siemens programmable logic controller (PLC) module and a self-written program (table S5). Each cycle consisted of two subcycles (Extraction 1 and Extraction 2, Fig. 3B) alternating between two rinse steps (Rinse 1 and Rinse 2, Fig. 3B). The extraction voltage and subcycle duration were set to 0.7 V and 110 min, respectively.

Lithium extraction from Dead Sea brine is hindered by its ultralow lithium content and abundance of interfering ions. To demonstrate the effectiveness of the pilot-scale DCMF process, mimic Dead Sea brines were used in this pilot-scale test because of the large amount (>10 tons) required. It was prepared based on the composition data in Table 1. As shown in Fig. 3C and fig. S9, 1 ton of mimic brine contains >400 kg of salt, with the fraction of LiCl equaling only 0.08%. The pilot-scale successfully extracted lithium from this harsh brine with a lithium recovery of 84.0% after eight cycles. Fig. 3D shows that the increment of lithium in the extraction compartment matches well with the decrement of lithium in the feed compartment, agreeing with the matter conservation. Thereafter, the brine feed was replaced, but the extraction solution was continuously used until a lithium concentration of 99.21 mM was reached after 112 cycles. The $LiFePO_4$/$FePO_4$ electrode voltage and external power were recorded using built-in voltmeters. As expected, the voltage between the $LiFePO_4$/$FePO_4$ electrodes was close to 0.825 V, whereas the external power provided 0.7 V (Fig. 3E). The average energy consumption of the $LiFePO_4$-$FePO_4$ electrode was 46011.16 J per cycle, with the contribution of external power determined as 38992.51 J according to Eq. 8:

$$W = U\int Idt \tag{8}$$

where $W$ (J) is the energy consumption, $U$ (V) is the voltage, $I$ (A) is the current, and $t$ (s) is the time.

The Ag/AgCl electrode acted as an internal power (i.e., osmotic energy) source, providing 7,008.29 J per lithium extraction cycle, which accounted for 15.23% of the overall energy consumption. The coulombic efficiency of each cycle (and hence, the extraction rate) was strongly positively correlated with the lithium concentration of the feed solution (Fig. 3E) and could be fully recovered after refreshing the feed, which indicated the robustness and sustainability of our process. No charge leakage was detected because (i) the external power could substantially suppress it and recover the original state of the electrodes and (ii) the physical isolation between the cathode and anode compartments suppressed electrode self-discharge (*32*–*34*).

Although the lithium concentration of extraction solution could be increased to the level (>3000 mM) by multiple cycles where lithium could be precipitated by the addition of $Na_2CO_3$ (as demonstrated in fig. S10, conducted by the bench-scale setup), it was stopped at about 99.21 mM during the pilot-scale test owing to time limitations. For simplicity, the extraction solution was concentrated using nanofiltration to primarily remove $Mg^{2+}$ and $Ca^{2+}$, enriched by reverse osmosis to ~1000.0 mM, and further concentrated to 3063.67 mM by solar evaporation. The solution pH was adjusted to 12.0 to precipitate trace amounts of $Mg^{2+}$ and $Ca^{2+}$, and a saturated $Na_2CO_3$ solution was then added to precipitate $Li_2CO_3$. The amount of the thus obtained $Li_2CO_3$ (3.175 kg) corresponded to an overall lithium recovery of 86.5%. The precipitate was subjected to x-ray diffraction and ICP-OES analyses. The x-ray diffraction pattern (Fig. 3F) matched that of the $Li_2CO_3$ standard (PDF#83-1454), and ICP-OES measurements revealed that $Na^+$, $K^+$, $Mg^{2+}$, and $Ca^{2+}$ were present at levels of 134.5, 9.1, 19.8, and 62.1 ppm, respectively, i.e., the obtained product met the standard of battery-grade $Li_2CO_3$ (YS/T582-2013).

### Discussion

Energy consumption and material costs were estimated based on the results of pilot-scale extraction and stability tests. The energy consumption of pilot-scale extraction was recorded and analyzed by using intelligent electric meters with R485 communication protocols (Table 2 and table S5). The total power consumption was only 70.43 W (1,183,289.79 J per cycle), i.e., 11.59 kilowatt-hours (kWh) were required to extract 1.0 kg of $Li_2CO_3$. The energy consumption directly related to lithium extraction was only 17.01% of the total energy consumption (1.97 kWh), including the power consumed by electrode rotation, solution loading and unloading, lithium adsorption, and electrode rinsing. Considering the value of 7008.29 J per cycle (i.e., 0.069 kWh per 1.0 kg of extracted $Li_2CO_3$), osmotic energy accounted for 3.48% of the energy consumption directly related to lithium extraction. The other 82.99% was consumed by the auxiliary system, including the control and rinsing systems. This proportion can be substantially decreased at a larger scale by optimizing the design of the auxiliary system and scale effects. For example, the control system comprises arithmetic logical units, instruction transmitters (electric relays), actuators, and monitors, with only the number of actuators

increasing proportionally with system size. Table S6 lists the rough estimates of itemized material and operation costs. The overall material and operation costs were determined to be ~5.89 US$ per kg of $Li_2CO_3$, indicating competitiveness with lithium extraction from lithium-rich resources ($2 to $9), and were lower than the average market price of $Li_2CO_3$ in 2022 to 2023 (~$70) (*35*, *36*).

We developed a DCMF cell design for lithium extraction from inferior brines, efficiently utilizing osmotic potential to decrease the energy consumption of the system. The extraction cost was competitive with that of lithium extraction from conventional resources, and the design was simple and easily upscalable. We expect the inherent process flexibility of our design to stimulate the integration of innovative ideas into broader applications.

## REFERENCES AND NOTES


1. G. Zubi, R. Dufo-López, M. Carvalho, G. Pasaoglu, *Renew. Sustain. Energy Rev.* **89**, 292–308 (2018).
2. Y. Huang, "Advancing the Sustainability of Batteries," A Tongji University/Nature Sustainability Expert Panel Report (Tongji University and Springer Nature, 2022).
3. G. Martin, L. Rentsch, M. Höck, M. Bertau, *Energy Storage Mater.* **6**, 171–179 (2017).
4. L. T. Peiró, G. V. Méndez, R. U. Ayres, *J. Miner. Met. Mater. Soc.* **65**, 986–996 (2013).
5. B. W. Jaskula, Lithium Statistics and Information, U.S. Geological Survey (United States Department of the Interior, 2022).
6. D. Castelvecchi, *Nature* **596**, 336–339 (2021).
7. J. Speirs, M. Contestabile, Y. Houari, R. Gross, *Renew. Sustain. Energy Rev.* **35**, 183–193 (2014).
8. C. B. Tabelin *et al*., *Miner. Eng.* **163**, 106743 (2021).
9. C. Liu *et al*., *Joule* **4**, 1459–1469 (2020).
10. A. Battistel, M. S. Palagonia, D. Brogioli, F. La Mantia, R. Trócoli, *Adv. Mater.* **32**, e1905440 (2020).
11. S. Yang, F. Zhang, H. Ding, P. He, H. Zhou, *Joule* **2**, 1648–1651 (2018).
12. Z. Zhao, X. Si, X. Liu, L. He, X. Liang, *Hydrometallurgy* **133**, 75–83 (2013).
13. M.-Y. Zhao *et al*., *Electrochim. Acta* **252**, 350–361 (2017).
14. Z.-Y. Guo, Z.-Y. Ji, J. Wang, X.-F. Guo, J.-S. Liang, *Desalination* **533**, 115767 (2022).
15. F. L. Mantia, M. Pasta, A. Battistel, German patent DE102012212770A1 (2012).
16. E. Julio, C. Marchini, worldwide patent WO2014047347A1 (2014).
17. Z. Li *et al*., *Energy Environ. Sci.* **14**, 3152–3159 (2021).
18. T. B. H. Schroeder *et al*., *Nature* **552**, 214–218 (2017).
19. W. Chen *et al*., *Adv. Mater.* **34**, e2108410 (2022).
20. H. T. Madsen, S. S. Nissen, J. Muff, E. G. Søgaard, *Desalination* **420**, 183–190 (2017).
21. Z. Zhang, L. Wen, L. Jiang, *Nat. Rev. Mater.* **6**, 622–639 (2021).
22. A. Siria, M.-L. Bocquet, L. Bocquet, *Nat. Rev. Chem.* **1**, 0091 (2017).
23. A. P. Straub, A. Deshmukh, M. Elimelech, *Energy Environ. Sci.* **9**, 31–48 (2016).
24. L. Wang, Z. Wang, S. K. Patel, S. Lin, M. Elimelech, *ACS Nano* **15**, 4093–4107 (2021).
25. B. Rausch, M. D. Symes, G. Chisholm, L. Cronin, *Science* **345**, 1326–1330 (2014).
26. A. Landman *et al*., *Nat. Mater.* **16**, 646–651 (2017).
27. H. Dotan *et al*., *Nat. Energy* **4**, 786–795 (2019).
28. E. Rodil, J. Vera, *Fluid Phase Equilib.* **187**, 15–27 (2001).
29. E. Rodil, J. Vera, *Fluid Phase Equilib.* **205**, 115–132 (2003).
30. A. Zelyanskii, L. Zhukova, G. Kitaev, *Inorg. Mater.* **37**, 523–526 (2001).
31. R. W. Clark, J. M. Bonicamp, *J. Chem. Educ.* **75**, 1182 (1998).
32. D. Brogioli *et al*., *Energy Environ. Sci.* **5**, 9870–9880 (2012).
33. X.-W. Han *et al*., *Renew. Energy* **218**, 119288 (2023).
34. M. C. Hatzell, R. D. Cusick, B. E. Logan, *Energy Environ. Sci.* **7**, 1159–1165 (2014).
35. A. Karrech, M. R. Azadi, M. Elchalakani, M. A. Shahin, A. C. Seibi, *Miner. Eng.* **145**, 106085 (2020).
36. C. Grosjean, P. H. Miranda, M. Perrin, P. Poggi, *Renew. Sustain. Energy Rev.* **16**, 1735–1744 (2012).
37. Z. Li *et al*., Lithium extraction from brine through a decoupled and membrane-free electrochemical cell design, version 1, Dryad (2024); https://doi.org/10.5061/dryad.k6djh9wg2.


## ACKNOWLEDGMENTS

We thank the Core Laboratories of KAUST for their support with characterization. **Funding:** Baseline Funds (BAS/1/1375-01); Competitive Research Fund under award no. URF/1/4713-01 from KAUST; KAUST Office of Sponsored Research (OSR) under award nos. ORA-2021-5096, OSR-CARF/CCF-3079, IED OSR-2019-4208, and CRG2019-4093. **Author contributions:** Conceptualization: Z.Li and Z.Lai; Data curation: Z.Li, I.-C.C., L.C., and X.L.; Formal analysis: Z.Li, I.-C.C., L.C., X.L., K.-W.H., and Z.Lai; Funding acquisition: K.-W.H., and Z.Lai; Investigation: Z.Li, I.-C.C., L.C., and X.L.; Methodology: Z.Li and Z.Lai; Project administration: K.-W.H. and Z.Lai; Visualization: Z.Li; Resources: K.-W.H. and Z.Lai; Supervision: K.-W.H. and Z.Lai; Validation: K.-W.H. and Z.Lai; Writing – original draft: Z.Li; Writing – review and editing: K.-W.H. and Z.Lai. **Competing interests:** A patent application based on the basic idea of this work has been filed. **Data and materials availability:** All data are available in the main text, supplementary materials, or the Dryad data repository (*37*). 

## SUPPLEMENTARY MATERIALS

science.org/doi/10.1126/science.adg8487
Materials and Methods
Figs. S1 to S13
Tables S1 to S6
References (*38*–*61*)
Movies S1 and S2

Submitted 25 January 2023; resubmitted 9 May 2024
Accepted 18 July 2024
10.1126/science.adg8487